Theor Chem Acc (2001) 107:15–21
DOI 10.1007/s002140100294

Theoretical
Chemistry Accounts

Regular article

Dual-level direct dynamics calculations of deuterium kinetic isotope effects for the Cl(2P) + C2H6 abstraction reaction

O. Roberto-Neto, F. B. C. Machado

Instituto de Estudos Avançados, Centro Técnico Aeroespacial, São José dos Campos, 12228–840, São Paulo, Brazil
Departamento de Química, Instituto Tecnológico de Aeronáutica, Centro Técnico Aeroespacial,
São José dos Campos, 12228–900, São Paulo, Brazil

Received: 6 June 2001 / Accepted: 12 July 2001 / Published online: 19 November 2001

Abstract. Kinetic isotope effects, KIEs, for hydrogen abstraction from C_2H_6 and C_2D_6 by chlorine atom have been studied by the dual-level direct dynamics approach. A low-level potential energy surface is obtained with the MNDO-SRP method. High-level structural properties of the reactants, transition state, and products were obtained at the MP2 level with the cc-pVDZ, aug-cc-pVDZ, and the cc-pVTZ basis sets. Using the variational transition state theory with microcanonical optimized multidimensional tunneling, the values of deuterium KIE, at 300 K, range from 2.28 to 3.27, in good agreement with the experimental values (2.69–5.88).

Key words: Variational transition state theory – Dual-level dynamics – Abstraction reaction – $Cl + C_2H_6$ – Kinetic isotope effect

Introduction

Abstraction of a hydrogen atom by chlorine is an important step in several reactions involving combustion and atmospheric chemistry of hydrocarbons, and has therefore attracted attention from both experimentalists [1] and theoreticians [2]. In the case of the $Cl(^2P) + C_2H_6 \rightarrow C_2H_5 + HCl$ abstraction reaction, its experimental investigation offers some difficulties because there are possible side reactions or non-adiabatic effects, which cause a departure from linear Arrhenius behavior at temperatures above 600 K [3]. The values for the rate coefficient at room temperature vary from 5.51×10^{-11} cm^3 molecule^{-1} s^{-1} [3] to 5.9×10^{-11} cm^3 molecule^{-1} s^{-1} [4]. This abstraction reaction is considered relatively fast, although its rate constants still fall below the values calculated using the simple collision theory [5]. Thus the barrier, although small, is not negligible.

Correspondence to: O. Roberto-Neto
e-mail: orlando@ieav.cta.br

It is challenging to obtain balanced calculations of the energetic features of a reaction with such a low barrier. For instance, this reaction is exothermic by −2.2 to −2.6 kcal mol^{-1} [6, 7], and it is almost barrierless with forward and reverse activation energies equal to 0.3 ± 0.2 kcal mol^{-1} [3] and 1 ± 1 kcal mol^{-1} [8], respectively. In a previous theoretical study [9], we have obtained the structures and energies of all stationary points (reactants, products, and transition state) using MP2 theory and the cc-pVDZ, aug-cc-pVDZ, cc-pVTZ, and aug-cc-pVTZ basis sets [10]. Single-point calculations at the MP2, QCISD(T), and CCSD(T) levels were also used to compute the energetic properties. We have also examined thermal rate constants for the forward reaction using the zero-order interpolated variational transition state theory (IVTST-0) approach [11].

Another important and difficult chemical kinetic property to be evaluated for hydrogen abstraction reactions [12] is the deuterium kinetic isotope effect (KIE) [13]. For the $Cl(^2P) + C_2D_6$ reaction, the experimental value of the deuterium KIE ranges from 2.69 to 5.88 [14, 15] at room temperature. As far as we know, no deuterium KIE values have been reported for the $C_2D_5 + DCl$ reverse reaction.

In this work, our main goal is to calculate thermal rate constants and deuterium KIEs by a dual-level approach to direct dynamics through the use of a semiempirical MNDO-SRP potential energy surface (PES). The MNDO-SRP method is a combination of MNDO general parameters [16] and specific reaction parameters (SRP) [17,18]. This method was chosen because ab initio calculations of the full PES are computationally too expensive. An alternative procedure is to make use of an analytical potential energy surface (APS) [19]. However, this method is not feasible for large polyatomic systems, because we need accurate and detailed data from the vibrational potential energy such as internal-coordinate couplings [20].

Bimolecular thermal rate constants and deuterium kinetic isotope effects were calculated using canonical variational transition state theory with interpolated corrections (VTST-IC) [20, 21] including multidimen-

sional tunneling corrections [22–25]. The C_2H_6/C_2D_6 KIE is defined in this paper as the ratio k_H/k_D, where k_H is the rate constant for unsubstituted ethane, and k_D is that for the isotopomer. When the value of the KIE is greater than unity it is called normal, otherwise it is called inverse [13].

Methods

In our previous paper [9], geometries, electronic energies, and harmonic vibrational frequencies for the perprotio reactants, transition state, and products were obtained at the MP2 level, using the cc-pVDZ, aug-cc-pVDZ, cc-pVTZ, and aug-cc-pVTZ Dunning basis sets [10]. These basis sets, for simplicity, were called for short b1, b2, b3, and b4, respectively. Complementing that study, values of the vibrational frequencies and moments of inertia for the per-deuterated stationary points are evaluated in this paper. The MP2 structural parameters were used to supply high-level information needed for VTST-IC, also called the dual-level direct dynamics method [20,21].

The set of specific reaction parameters for the MNDO-SRP method were developed by trial-and-error [26] to provide a better description of selected structural and energetic properties for the full potential energy surface. The properties used in the optimization process of the semiempirical parameters are forward classical barrier height ($\Delta V_f^{\ddagger}$), vibrationally adiabatic barrier height ($\Delta V_a^{G,\ddagger}$), geometry of the transition state, values of representative tunneling energies along the reaction coordinate, and Arrhenius activation energy calculated by a two-point fit at 300 K and 400 K. The calculated values of the small and large representative tunneling energies, in all ranges of temperatures, were used to guide the optimization process of the semiempirical parameters because their smooth variations are, in general, related to a suitable description of the reaction-path curvature. The best values for the forward classical barrier height and for the energy of reaction were set to 4.4 and 2.9 kcal mol^{-1}, respectively.

According to the dual-level notation [20,21], a calculation which uses MP2/cc-pVDZ (high-level) and MNDO-SRP (low-level) methods is called MP2/cc-pVDZ///MNDO-SRP-IC. In a shorter notation, this level of calculation is called MP2/b1///MNDO-SRP. Calculations with the remaining basis sets are denoted similarly. Ab initio calculations were evaluated with the GAUSSIAN 98 code [27].

The reaction path was calculated in mass-weighted rectilinear Cartesian coordinates, using the Page and McIver's method [28] with a step size of 0.01 a_0. The Hessian matrix was calculated at every step along this reaction path. The reaction coordinate, *s*, along the minimum energy path (MEP) is defined as the signed distance from the saddle point, with $s > 0$ corresponding to the product direction. The units of *s* are bohr, and all calculations are carried out in mass-scaled coordinates with a reduced mass μ equal to 1 amu. We use the interpolated-corrections-additive algorithm method (ICA) [20,21] to interpolate corrections on the low-level surface.

In transition state theory (TST) and canonical variational transition state theory (CVT) [22] calculations, the symmetry factors used are 6 and 1 for the forward and reverse reactions, respectively. We have included the two low-lying fine structure electronic states, $^2P_{1/2}$ and $^2P_{3/2}$, in the calculations of the electronic partition functions, which are separated by 882 cm^{-1}, to account for spin-orbit coupling [29].

Finally, we considered the tunneling corrections. We use the microcanonically optimized multidimensional tunneling (μOMT) approach [25], in which, at each total energy, the larger of the SCT and LCT tunneling probabilities is taken as the best estimate. The unidimensional method of Wigner [30] as well as the zero-curvature tunneling [23] and small-curvature tunneling [24] methods are also employed in the analysis of the deuterium KIE. All dual-level rate constants were carried out with MORATE 8.5 code [31], which is an interface between MOPAC 5.09 mn [32] and the POLYRATE 8.5 code [33].

Results and discussion

Properties of the potential energy surface

The values of the classical barrier height ($\Delta V_f^{\ddagger}$) and vibrationally adiabatic barrier height ($\Delta V_a^{G,\ddagger}$), evaluated at the saddle point, and the electronic energy of the reaction (ΔE) and enthalpy of reaction at 0 K (ΔH_0) are listed in Table 1. Results from our previous paper [9] are also summarized in Table 1. The MP4/b3//MP2/b3, QCISD(T)/b3//MP2/b3, and CCSD(T)/b3//MP2/b3 calculations provide values for the forward adiabatic barriers equal to −0.1, −0.4, and −0.3 kcal mol^{-1}, respectively. These results are close to the experimental activation energy of 0.3 kcal mol^{-1}. In the previous study we have also applied an empirical procedure [26] to obtain the forward classical barrier and the activation energy. Using the IVTST-0 method, the best fit yields a forward activation energy of 0.3 kcal mol^{-1} and a classical barrier height of 4.4 kcal mol^{-1}, which is in good agreement with the MP4 (4.3 kcal mol^{-1}), QCISD(T) (4.0), and CCSD(T) (4.1 kcal mol^{-1}) results using the MP2/b3 geometries and frequencies. The MP2/b4 calculations give values for the electronic energy of reaction and vibrationally adiabatic barrier height equal

Table 1. Energetic properties (in kcal mol^{-1}) of the $Cl(^2P) + C_2H_6$ reaction

Method	$\Delta V_f^{\ddagger}$	$\Delta V_a^{G,\ddagger}$	ΔE	ΔH_0
AM1	−8.2		−18.0	
PM3	−12.4		−14.0	
MNDO	3.1	−1.2	−11.7	−11.7
MNDO-SRP	4.4	0.1	−6.0	−7.3
MP2/b4[a]	0.7	−3.7	2.9	−2.4
MP4/b3//MP2/b3[a]	4.3	−0.1	5.5	0.1
QCISD(T)//b3/MP2/b3[a]	4.0	−0.4	5.3	−0.1
CCSD(T)//b3/MP2/b3[a]	4.1	−0.3	5.3	−0.1
empirically adjusted[b]	4.4	0.3		
Expt.		0.3 ± 0.2[c]		−(2.2–2.6)[d]

[a] [9]
[b] [9] and see also the discussion in the text
[c] [3]
[d] [6, 7]

to 2.9 and −2.4 kcal mol^{-1}, respectively. Therefore, at this level of the theory there is a close agreement with the experimental enthalpy of reaction which range from −2.2 to −2.6 kcal mol^{-1} [6,7]. Based on these previous results, the values of the energetic parameters used as high-level data in the VTST-IC calculations are set as 4.4 kcal mol^{-1} for the forward classical barrier height and 2.9 kcal mol^{-1} for the electronic energy of the reaction.

Comparing all available semiempirical methods for their predictions of energetic parameters, we found that the MNDO Hamiltonian gives the best agreement with the high-level data, and thus it was chosen for our reparametrization procedure. In the final process of optimization of the MNDO semiempirical parameters, only the Upp and βs (resonance integrals) for carbon, and the U_{ss} parameter for chlorine atom were modified. The new set of MNDO-SRP parameters are changed by −3%, 2%, and 5%, respectively, from their original values [16]. The MNDO-SRP values of $\Delta V_f^{\ddagger}$ (4.4 kcal mol^{-1}) and $\Delta V_a^{G,\ddagger}$ (0.1 kcal mol^{-1}) are in close agreement with the high-level predictions, i.e., 4.4 kcal mol^{-1} and 0.3 kcal mol^{-1}, respectively (Table 1). Note that the MNDO-SRP enthalpy of reaction (−7.3 kcal mol^{-1}) is still too negative, but is corrected in the VTST-IC procedure of interpolation [20, 21].

Structural parameters of the transition state structure (symmetry C_s) (Fig. 1) are listed in Table 2. The MNDO-SRP values of the C-H bond lengths are slightly overestimated in relation to the MP2 results using the b1, b2, and b3 basis sets. The MNDO-SRP method gives C2-H8 (broken bond) and H8-Cl (formed bond) bonds with practically the same distance, which is an indication of a symmetrical curve at the top of the potential. The abstraction angle (C2H8Cl) is predicted to be almost collinear in the MNDO-SRP calculations (179.6°), and therefore is in reasonable agreement with the MP2 calculations.

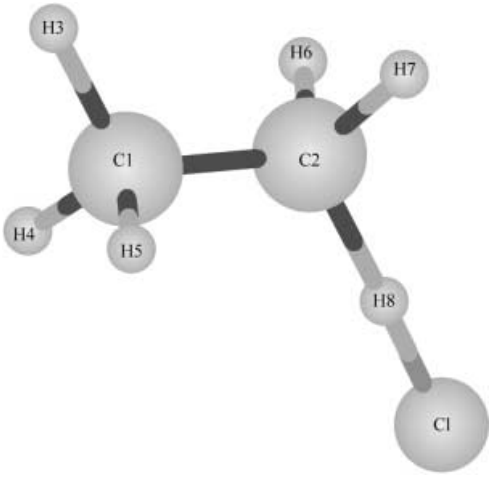

Fig. 1. Transition state structure, C_2H_6Cl (symmetry C_s)

In our previous paper [9], perprotio harmonic frequencies at MP2/b1, MP2/b2, and MP2/b3 levels were evaluate for the $Cl + C_2H_6$ reaction, and the transition state was identified as first-order because its Hessian matrix has only one negative eigenvalue. In this present study, we evaluated the analytical gradients for the perdeuterated stationary points at the same levels as previous calculations, as well as using the MNDO and MNDO-SRP methods. The imaginary frequency gives information of the shape of the potential, and therefore is an important parameter to be adjusted in a dual-level study. The MP2 harmonic frequencies of the perdeuterated transition states (Table 3) obtained with the b1, b2, and b3 basis sets are equal to 780i, 670i, and 692i cm^{-1}, respectively, while the MNDO method predicts a higher value (935i cm^{-1}). However, calculations at MNDO-SRP level improve the MNDO results and they give values for the imaginary frequency (755i cm^{-1}) and for the zero-point vibrational frequency (33.1 kcal mol^{-1}) in better agreement with the high-level data.

Classical potential along the MEP, $V_{MEP}(s)$, and the vibrationally adiabatic ground-state potential curve, $\Delta V_a^G(s)$, which is the sum of V_{MEP} and ZPVE (zero-point vibration energy), as a function of *s* are plotted in Fig. 2. A glance at Fig. 2 shows that the ΔV_a^G potential has dips symmetrically localized on both sides of the saddle point.

An analysis of the orthogonal modes around the saddle point shows that various vibrational modes are coupled with the reaction path in the range of −0.1 to 0.1 a_0. Absolute values of the coupling terms, $|B_{mF}|$ (*s*), [22] (Table 4) are calculated using both the original VTST algorithm, which takes the variational dividing surface as a hypersurface normal to the gradient [20], and employing the reorientation of the dividing surface (RODS) algorithm [34, 35]. In the text, the original VTST algorithm is called normal dividing surface (NDS). The RODS method is used to extract a stable

Table 2. Values of the bond distances (in Å) and angles (in degrees) for the transition state structure

Parameter	MP2/b1	MP2/b2	MP2/b3	MNDO	MNDO-SRP
C1–C2	1.502	1.505	1.485	1.503	1.502
C1–H3	1.105	1.103	1.086	1.112	1.113
C1–H4	1.099	1.097	1.081	1.109	1.108
C2–H6	1.097	1.095	1.077	1.099	1.092
C2–H8	1.358	1.315	1.330	1.337	1.476
H8–Cl	1.464	1.499	1.464	1.517	1.463
C2C1H3	109.7	109.1	109.7	109.6	108.5
C2C1H4	111.3	111.3	111.3	111.7	112.4
C1C2H6	117.0	116.7	117.3	100.3	98.0
C1C2H8	105.2	105.3	107.9	108.2	108.3
C2H8Cl	175.6	176.9	176.6	180.0	179.6

Table 3. Vibrational frequencies (in cm^{-1}) and zero-point vibrational frequencies, ZPVE, (in kcal mol^{-1}) for the transition state (C_2D_6Cl)

Mode	MP2/b1	MP2/b2	MP2/b3	MNDO	MNDO-SRP
1a″	2429	2410	2426	2478	2489
2a″	2382	2363	2376	2432	2443
3a′	2347	2326	2341	2413	2415
4a′	2294	2277	2312	2404	2401
5a′	2217	2201	2235	2387	2371
6a′	1220	1208	1231	1353	1363
7a″	1084	1083	1100	1112	1121
8a′	1062	1066	1083	1084	1097
9a′	1060	1058	1077	1051	1072
10a′	994	986	1007	1041	1066
11a″	983	976	1001	950	956
12a′	907	904	918	920	917
13a″	735	751	754	776	756
14a′	717	749	747	718	631
15a″	590	601	613	634	614
16a′	585	598	607	580	501
17a′	441	419	440	456	496
18a′	297	322	326	238	245
19a′	120	140	131	118	120
20a′	105	114	118	94	69
21a′	780i	670i	692i	935i	755i
ZPVE	32.3	32.2	32.7	33.2	33.1

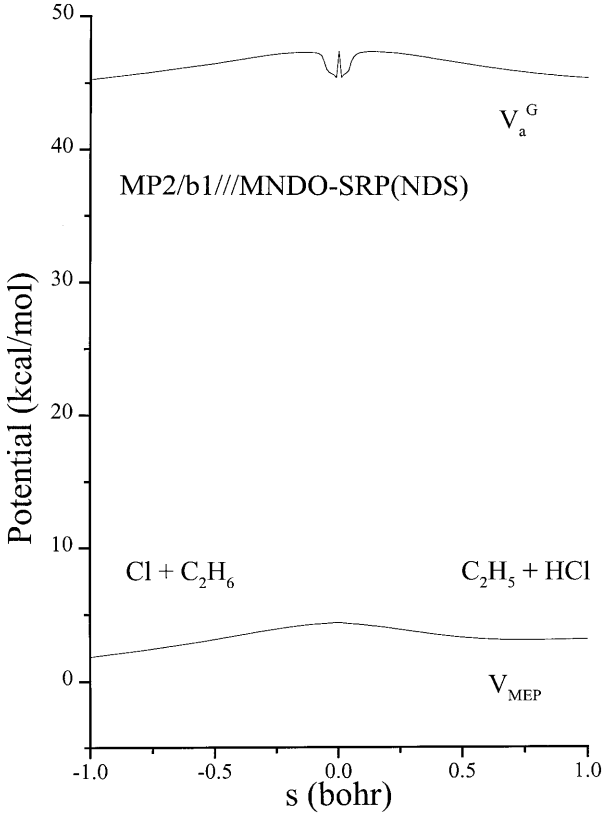

Fig. 2. Classical potential energy-curve (V_{MEP}) and vibrationally adiabatic ground-state potential curve (ΔV_a^G) as a function of reaction coordinate s calculated using the original VTST algorithm

CVT free energy of activation from an unstable or not well-converged MEP [34, 35]. Calculations using the original VTST method give high values for the B_{5F}, B_{6F}, and B_{10F} coupling terms at values of s equal to −0.01, −0.06, and −0.05 a_0, respectively. These high values of coupling terms between the reaction path and the orthogonal modes are caused by the sudden variation of the gradients at the flat region of the saddle point. However, calculations using the RODS algorithm eliminate these unphysical perturbations on the generalized frequencies (Table 4), and they give a smooth variation of the ΔV_a^G potential (Fig. 3). The maximum of the ground-state vibrationally adiabatic potential curve appears at $s = -0.001$, thus with a negligible variational shift.

To complement this study, generalized normal-mode vibrational frequencies along the MEP are shown in Fig. 4. At the asymptotic limit of the reactants, the $5a_1$ and $6a_1$ modes correspond to the C-H stretching modes of C_2H_6 [36]. The reactive $6a_1$ mode suffers a sharp variation near the saddle point, as is typical of hydrogen transfer reactions [20]. It is directly involved in the hydrogen transfer and with the H-Cl stretching mode at the products side. The other $5a_1$ modes stay practically constant along the reaction path. Finally, the two lowest frequencies $19a_1$ and $20a_1$ are the transition modes, and they are imaginary along the MEP. As discussed elsewhere [21, 37], this may occur because of the unphysical nature of the Cartesian coordinate system. Therefore, these transition modes were interpolated directly from the frequencies at the transition state, reactants, and products using the IVTST-0 approach [21].

Rate constants and KIE

We have previously found [9] that, despite the low value of the forward activation barrier (0.3 ± 0.2 kcal mol^{-1}), unidimensional tunneling effects are important for the evaluation of the thermal rate constants. In this study, using a full potential energy surface we found that large corner cutting tunneling effects dominated most of the reaction path. Thus, our reported CVT rate constants

Table 4. Absolute values of the reaction-path curvature components B_{mF} (in a_0^{-1}) vs the arc length along the reaction coordinate for modes 5, 6, 10, and 12

s(a_0)	NDS[a]				RODS[b]			
	$\|B_{5F}\|$	$\|B_{6F}\|$	$\|B_{10F}\|$	$\|B_{12F}\|$	$\|B_{5F}\|$	$\|B_{6F}\|$	$\|B_{10F}\|$	$\|B_{12F}\|$
−0.10	0.00	1.87	1.28	1.00	0.00	1.84	0.05	0.01
−0.09	0.00	1.72	2.67	1.72	0.00	1.68	0.02	0.07
−0.08	0.00	1.50	6.02	3.08	0.01	1.44	1.72	0.19
−0.07	0.00	1.08	12.90	5.46	0.48	0.39	1.30	0.79
−0.06	0.02	0.48	19.52	8.62	0.03	0.09	0.58	0.70
−0.05	0.02	0.15	14.7	10.99	0.15	0.04	0.10	0.65
−0.04	0.51	0.02	6.31	8.51	0.48	0.03	0.05	0.04
−0.03	2.24	0.04	2.83	5.34	0.48	0.05	0.06	0.04
−0.02	7.66	0.05	1.58	3.42	0.02	0.00	0.09	0.24
−0.01	11.94	0.29	0.97	2.30	0.02	0.24	0.91	0.31
0.01	6.71	0.46	0.14	0.06	0.03	0.20	0.90	0.10
0.02	7.30	0.37	1.58	3.50	0.03	0.70	1.05	0.18
0.03	2.20	0.11	2.84	5.44	0.08	0.11	0.22	0.03
0.04	0.59	0.26	6.48	8.38	0.20	0.12	0.35	0.21
0.05	0.08	0.57	12.93	8.80	0.09	0.30	0.49	0.06
0.06	0.02	1.13	13.72	5.86	0.17	1.05	0.85	0.29
0.07	0.02	1.80	10.13	3.78	0.00	1.73	0.33	0.22
0.08	0.01	2.20	6.44	2.52	0.00	1.82	0.03	0.12
0.09	0.01	2.30	3.93	1.72	0.00	1.94	0.00	0.06
0.10	0.00	2.27	2.41	1.20	0.00	1.90	0.02	0.03

[a]Normal diving surface
[b]Reorientation of the dividing surface

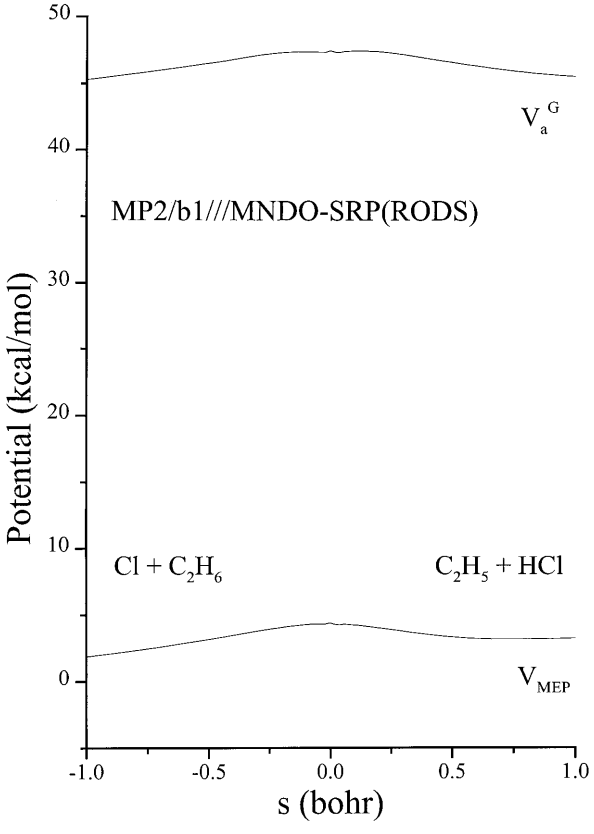

Fig. 3. Classical potential energy-curve (V_{MEP}) and vibrationally adiabatic ground-state potential curve (ΔV_a^G) as a function of reaction coordinate *s* calculated using the RODS algorithm

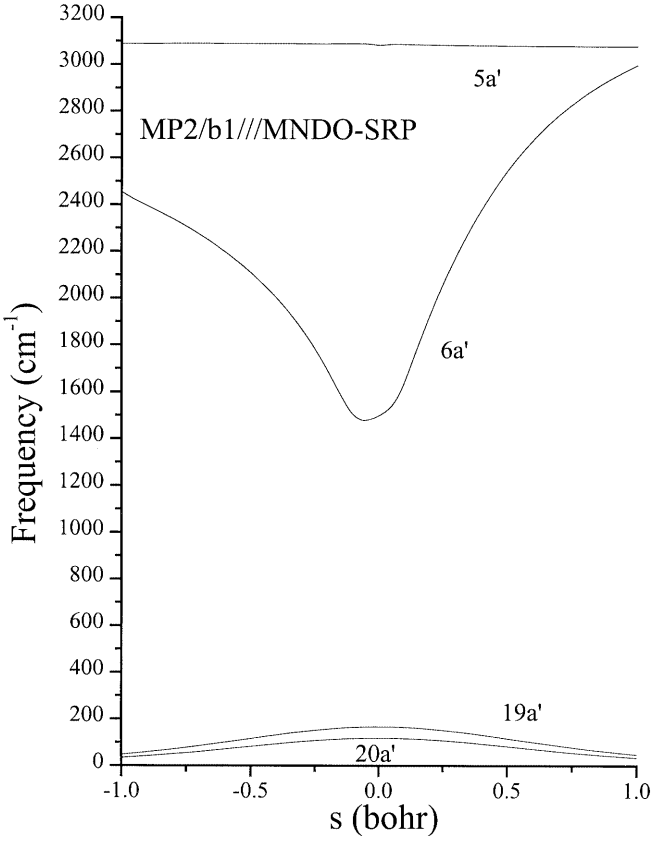

Fig. 4. Selected generalized normal-mode vibrational frequencies as a function of reaction coordinate *s* calculated using the RODS algorith

for the $Cl(^2P) + C_2H_6$ reaction (Table 5) include microcanonical optimized multidimensional tunneling correction (μOMT) [25]. In general, the CVT/μOMT calculations agree with experiment within a maximum factor of 4. The results also show that there are sensitive differences in the values of rate constants when the

Table 5. CVT/μOMT rate constants for the $Cl(^2P) + C_2H_6$ abstraction reaction

T(K)	MP2/b1	MP2/b2	MP2/b3	Exp.[a]	Exp.[b]
250	1.6(−11)[c]	1.0(−11)	1.0(−11)	5.0(−11)	5.5(−11)
300	1.9(−11)	1.2(−11)	1.1(−11)	5.5(−11)	5.9(−11)
350	2.2(−11)	1.5(−11)	1.4(−11)	5.9(−11)	6.2(−11)
400	2.5(−11)	1.8(−11)	1.6(−11)	6.1(−11)	6.4(−11)
500	3.41(−11)	2.5(−11)	2.3(−11)	6.6(−11)	6.7(−11)
600	4.6(−11)	3.4(−11)	3.1(−11)	7.1(−11)	6.9(−11)
800	7.7(−11)	5.9(−11)	5.3(−11)	8.2(−11)	7.2(−11)
1000	1.2(−10)	9.2(−11)	8.2(−11)		
1500	2.7(−10)	2.1(−10)	1.9(−10)		

[a] [4]
[b] [3]
[c] 1.6(−11) stands for 1.6×10^{-11} in cm^3 $molecule^{-1}$ s^{-1}

MP2/b1, MP2/b2, and MP2/b3 structural properties are used as high-level corrections in the dual-level calculations.

In a previous study of the C_2H_6/C_2D_6 KIE, Tschuikow-Roux et al. [14] have computed the so-called theoretical maximum isotope effect equal to 8, which is too large when compared to the experimental values (2.69–5.88) [14, 15]. That theoretical estimation of the KIE is based on a one-dimensional three-particle model which ignores any tunneling correction [14]. In the present study, we have calculated the deuterium KIE using several levels for estimating the semi-classical tunneling contributions (Table 6). At the MP2/b3///MNDO-SRP level, the values of KIE increase in relation to the conventional TST calculations using the unidimensional tunneling approximation of Wigner [30]. These results are similar to those ones found in the $Cl + CH_4$ abstraction reaction [38]. CVT calculations of the deuterium KIE do not change the results in relation to TST method because the dual-level surfaces do not predict variational shift. The importance of multidimensional tunneling corrections is shown by a consistent improvement in the values of KIE obtained at the ZCT, SCT, and μOMT levels. At the MP2/b3///MNDO-SRP level, the values of deuterium KIE are equal to 8.33, 6.74, and 2.28 using the ZCT, SCT, and μOMT methods of multidimensional tunneling corrections (Table 6). At 300 K, the values of deuterium KIE calculated with the μOMT multidimensional method (Table 7) range from 2.21 to 3.27, in good agreement with the experimental values (~2.69–5.88) [14,15]. Note that the similar $Cl(^2P) + CH_4$ abstraction reaction presents higher values of deuterium KIE, (~11–18) [2]. The Cl $(^2P) + C_2H_6$ abstraction reaction also show normal values for deuterium KIE (>1) in the range of 250–1500 K.

Conclusions

Dual-level direct dynamics calculations for the $Cl(^2P) + C_2H_6 \rightarrow C_2H_5 + HCl$ abstraction reaction were carried out using a low-level MNDO-SRP surface. Structural and energetic properties of the stationary points, used in the interpolated corrections, were obtained by employing the MP2 method and several correlation consistent polarized-valence basis sets of Dunning. Variational transition state theory with microcanonical optimized multidimensional tunneling contributions was employed to obtain thermal rate constants and deuterium kinetic isotope effects (KIEs). Computed rate constants in the range 250–1500 K differ from experiment by, at most, a factor of 3.6 using the MP2/cc-pVDZ///MNDO-SRP-IC method. At 300 K, the calculated values of the KIE obtained using the cc-pVDZ, aug-cc-pVDZ, and cc-pVTZ basis sets are equal to 3.27, 2.21, and 2.28, respectively, in good agreement with the experimental values (~2.69–5.88) [14,15]. We hope these calculations will be useful for advancing the understanding and accurate modeling of the chemical kinetics of atmospheric and combustion reactions involving chlorine and hydrocarbons or other species containing C-H bonds.

Table 6. MP2/b3///MNDO-SRP values of the C_2H_6/C_2D_6 KIE

T(K)	TST	TST/W	CVT	ZCT	SCT	μOMT
250	17.67	22.63	17.69	12.14	7.10	2.36
300	10.86	13.26	10.90	8.33	6.74	2.28[a]
350	7.64	8.97	7.65	6.25	5.33	2.19
400	5.83	6.66	5.84	4.98	4.40	2.10
500	3.98	4.37	3.98	3.58	3.30	1.95
600	3.08	3.32	3.09	2.86	2.70	1.82
800	2.27	2.36	2.27	2.17	2.10	1.65
1000	1.91	1.96	1.91	1.85	1.81	1.55
1500	1.57	1.59	1.57	1.55	1.53	1.42

[a] Experimental (2.69–5.88) [14,15]

Table 7. CVT/μOMT values of the C_2H_6/C_2D_6 KIE

T(K)	MP2/b1	MPb2/b2	MP2/b3
250	3.65	2.29	2.36
300	3.27	2.21	2.28[a]
350	2.97	2.13	2.19
400	2.73	2.05	2.10
500	2.37	1.91	1.95
600	2.13	1.80	1.82
800	1.83	1.65	1.65
1000	1.67	1.55	1.55
1500	1.48	1.44	1.42

[a] Experimental (2.69–5.88) [14,15]

Acknowledgements. The authors are grateful to Professor D.G. Truhlar for providing the MORATE and POLYRATE codes, and for his helpful discussions and suggestion of using the RODS method. The authors also thank P.L. Fast for his assistance with RODS calculations. Financial support from Conselho Nacional de Desenvolvimento Científico e Tecnológico (CNPq), and Fundação de Amparo à Pesquisa do Estado de São Paulo (FAPESP), and computational facilities of the Centro Nacional de Computação Científica de Alto Desempenho de Campinas-SP (CENAPAD-SP) are also gratefully acknowledged.

References

1. Crowley JN, Saueressig G, Bergamashi P, Fisher H, Harris GW (1999) Chem Phys Lett 303: 268
2. Corchado JC, Truhlar DG, Espinosa-García J (2000) J Chem Phys 112: 9375

3. Pilgrim JS, McIlroy A, Taatjes CA (1997) J Phys Chem A 101: 1873
4. Atkinson R, Baulch DL, Cox RA, Hampson RF Jr, Kerr JA, Troe J (1992) J Phys Chem Ref Data 21: 1125
5. Benson SW, Dobis O (1998) J Phys Chem A 102: 5175
6. Catellano AL, Marriott PR, Griller DJ (1981) J Am Chem Soc 103: 4262
7. Lide DR (ed) (1994) CRC Handbook of chemistry and physics. CRC Press, Boca Raton
8. Parmar SS, Benson SW (1989) J Am Chem Soc 111: 57
9. Roberto-Neto O, Machado FBC (2001) J Mol Struct (Theochem) (in press)
10. Dunning TH Jr (1989) J Chem Phys 90: 1007
11. Gonzalez-Lafont A, Truong TN, Truhlar DG (1991) J Chem Phys 95: 8875
12. Kurosaki Y, Takaynagi T (2000) J Chem Phys 113: 4060
13. Melander L, Saunders WH Jr (1980) Reaction rates of isotopic molecules, 2nd edn. Wiley-Interscience Publication, New York
14. Tschuikow-Roux E, Niedzielski J, Faraji F (1985) Can J Chem 63: 1093
15. Dobbis O, Benson SW, Mitchell TJ (1994) J Phys Chem 98: 12,284
16. Dewar MJS, Rzepa HS (1978) J Am Chem Soc 100: 784
17. Gonzalez-Lafont A, Truong TN, Truhlar DG (1991) J Phys Chem 95: 4618
18. Rossi I, Truhlar DG (1995) Chem Phys Lett 233: 231
19. Truhlar DG, Steckler R, Gordon MS (1987) Chem Rev 87: 217
20. Truhlar DG (1995) In: Heidrich D (ed) The reaction path in chemistry: current approaches and perspectives. Kluwer, Dordrecht, The Netherlands, p 229 and references cited therein
21. Wu WP, Liu YP, Truhlar DG (1994) J Chem Soc Faraday Trans 90: 1715
22. Truhlar DG, Isaacson AD, Garrett BC (1985) In: Baer M (ed) The theory of chemical reaction dynamics. CRC Press, Boca Raton, vol 4, p 65
23. Garrett BC, Truhlar DG, Grev RS, Magnuson AW (1980) J Phys Chem 84: 1730
24. Liu YP, Lynch GC, Truong TN, Lu DH, Truhlar DG (1993) J Am Chem Soc 115: 2408
25. Liu YP, Lu DH, González-Lafont A, Truhlar DG, Garrett BC (1993) J Am Chem Soc 115: 7806
26. Corchado JC, Espinosa-Garcia J, Roberto-Neto O, Chuang YY, Truhlar DG (1998) J Phys Chem A 102: 4899
27. Frisch MJ, Trucks GW, Schlegel HB, Scuseria GE, Robb MA, Cheeseman JR, Zakrzewski VG, Montgomery JA Jr, Stratmann RE, Burant JC, Dapprich S, Millam JM, Daniels AD, Kudin KN, Strain MC, Farkas O, Tomasi J, Barone V, Cossi M, Cammi R, Mennucci B, Pomelli C, Adamo C, Clifford S, Ochterski J, Petersson GA, Ayala PY, Cui Q, Morokuma K, Malick DK, Rabuck AD, Raghavachari K, Foresman JB, Cioslowski J, Ortiz JV, Stefanov BB, Liu G, Liashenko A, Piskorz P, Komaromi I, Gomperts R, Martin RL, Fox DJ, Keith T, Al-Laham MA, Peng CY, Nanayakkara A, Gonzalez C, Challacombe M, Gill PMW, Johnson B, Chen W, Wong MW, Andres JL, Gonzalez C, Head-Gordon M, Replogle ES, Pople JA (1998) Gaussian 98, Revision A7. Gaussian Inc, Pittsburgh PA
28. Page M, McIver JW Jr (1988) J Chem Phys 88: 922
29. Moore CE (1971) Atomic energy levels. Nat Stand Ref Data Ser. National Bureau of Standards (US), vol II
30. Wigner EP (1932) Z Phys Chem Abt B 19: 203
31. Chuang YY, Fast PL, Hu WP, Lynch GC, Liu YP, Truhlar DG (2000) MORATE, Version 8.5, University of Minnesota, Minneapolis
32. Stewart JJP, Rossi I, Hu WP, Lynch GC, Liu YP, Chuang YY, Li J, Cramer CJ, Fast PL, Truhlar DG (1999) MOPAC version 5.09 mn, University of Minnesota, Minneapolis
33. Corchado JC, Chuang YY, Fast PL, Villà V, Hu WP, Li YP, Lynch GL, Nguyen KA, Jackels C, Melissas VS, Lynch J, Rossi I, Coitiño EL, Ramos AF, Steckler R, Garrett BC, Isaacson AD, Truhlar DG (2000) POLYRATE version 8.5, University of Minnesota, Minneapolis
34. Villà J, Truhlar DG (1997) Theor Chem Acc 97: 317
35. González-Lafont A, Villá J, Lluch JM, Bertrán J, Steckler R, Truhlar DG (1998) J Phys Chem A 102: 3420
36. Urban J, Schreiner PR, Vacek G, Scheyer PR, Huang JQ, Leszczynski J (1997) Chem Phys Lett 264: 441
37. Chuang YY, Truhlar DG (1997) J Chem Phys 107: 83
38. Roberto-Neto O, Coitiño EL, Truhlar DG (1998) J Phys Chem A 102: 4568